

Fatigue Behaviour of a Sharply Notched Carbon Steel under Torsion

B. Atzori¹, P. Lazzarin² and M. Quaresimin²

¹ University of Padova, Department of Mechanical Engineering, Via Venezia 1, 35131 Padova (Italy). E-mail: bruno.atzori@unipd.it

² University of Padova, Department of Management and Engineering, Stradella S. Nicola 3, 36100 Vicenza (Italy).
E-mail: paolo.lazzarin@unipd.it, marino.quaresimin@unipd.it

ABSTRACT. *The paper deals with fatigue strength properties and damage modes of a C40 carbon steel (normalised state) subjected to fully reversed torsion. Both smooth and notched specimens with four different V-shaped notches are tested. In all notched specimens the notch tip radius r is kept constant and equal to 0.5 mm while the notch depth changes from geometry to geometry. Fatigue crack nucleation and propagation phases are discussed in detail as well as the influence of microstructure on low/high cycle fatigue behaviour.*

INTRODUCTION

Fatigue threshold behaviour under mode III and in-phase mixed mode III and I loading conditions has extensively been studied by using V-notches, slit and fatigue pre-cracked specimens [1-8]. Nevertheless, understanding of the phenomenon is far less advanced with respect to mode I and a working definition analogous to mode I is difficult to establish. The practical difficulties of mode III threshold testing mainly depend on [5]:

- mode transition, for example from mode III to mode I, which occurs long before crack arrest. Different proposals were therefore made to define fatigue thresholds in terms of this transition. However, thresholds thus defined are no longer comparable to those defined in Mode I, since the cracks do not arrest, but continue to grow in a different way;
- the extensive plastic zone which can be generated in small test specimens;
- the problem of crack surface interference and load dissipation on crack flanks. Comparison of mode III fatigue threshold results using various type of pre-defects shows that slit specimens give lower threshold values, compared to specimens pre-cracked in tension. On the other hand, V-notched specimens, despite being finished with the same notch root radius as the slit specimens, give higher threshold values than those obtained using pre-cracked specimens [5].

The problem might be even more complex under fatigue conditions different from those of fatigue threshold. The paper summarises fatigue strength data obtained from standard

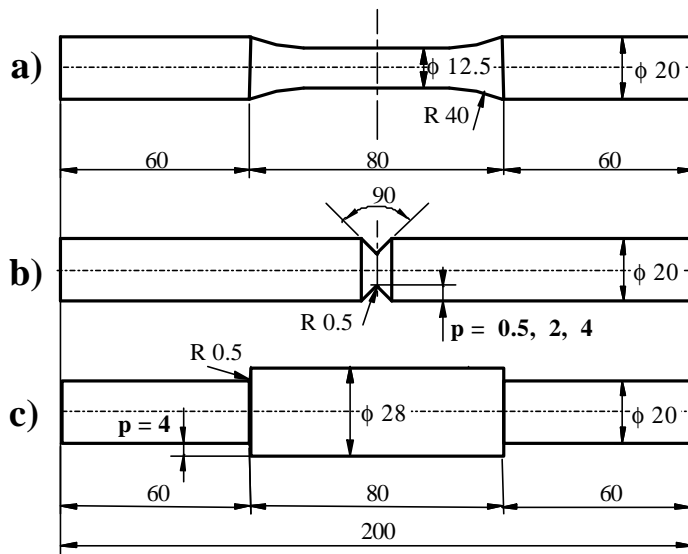


Figure 1. Geometry of the specimens.

fully reversed torsion tests carried out on V-shaped specimens, all characterised by a notch tip radius equal to 0.5 mm.

Fatigue crack nucleation and propagation phases are analysed in detail by means of optical and electronic microscopy. Despite the differences due to notch shape and load level, all fatigue strength data are summarised in terms of the Notch Stress Intensity Factor (N-SIF). Such factors are calculated on the basis of the stress distribution related to the uncracked

geometry, the notch being modelled simply as a re-entrant corner. N-SIF includes the influence of notch dept and the size effect. Despite the complexity of the fatigue phenomena, N-SIF are seen able to summarise the fatigue strength data in a single band with a very limited scatter. This makes the N-SIF a useful and powerful tool in fatigue life assessments in the presence of small value of the notch tip radius.

MATERIAL AND GEOMETRY OF SPECIMENS

The geometry of smooth and notched specimens is shown in Fig. 1. With reference to V-shaped notches (Fig. 1b), the V-notch depth ranges from 0.5 to 4 mm. The height of the shoulder (Fig. 1c) is 4.0 mm. In all notched specimens the notch tip radius was kept constant and equal to 0.5 mm. Such a value makes it difficult any correlation between the theoretical stress concentration factor K_t and the fatigue strength reduction factor K_f , since the notch sensitivity index exhibits a large scatter. Finite element analyses carried out by using the ANSYS® code gave a theoretical stress concentration factor (referred to the net area) equal to 1.94, 2.03 and 1.73 for the symmetric V-notches with a depth equal to 4.0 mm, 2.0 mm and 0.50 mm, respectively. On the other hand, the geometry with shoulders is characterised by a $K_{t,net} = 1.82$.

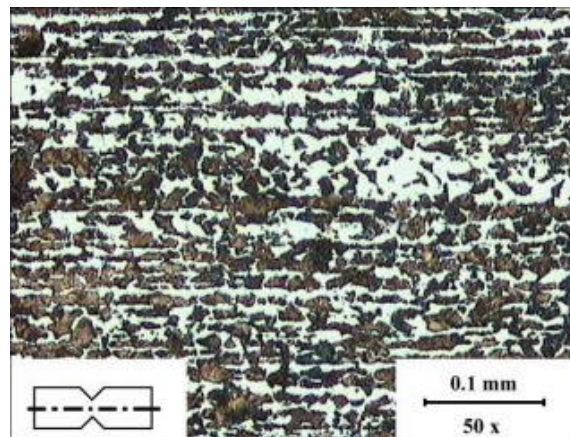


Figure 2. Microstructure of the C40 steel (normalised state).

Table 1. Tensile properties of the C40 carbon steel (normalized state).

| E [MPa] | $\sigma_{p0.2}$ [MPa] | σ_u [MPa] |
|---------|-----------------------|------------------|
| 206000 | 537 | 715 |

In parallel, microstructural analyses showed that, due to the normalisation treatment, two phases are present: ferrite (white zones in Fig. 2) and pearlite (black zones). Due to the drawing process used to obtain the bars, the two phases are forced to dispose in alternate bands whose main direction coincides with the specimen longitudinal axis. As discuss later, early phases of fatigue damage evolution have been strongly influenced by the particular microstructure.

Fatigue Tests

Before being fatigue tested, all specimens were polished in order both to eliminate any surface scratch or mark due to machine tools and make the analysis of fatigue crack evolution easier. Fatigue tests were carried out by means of a MTS 809 servohydraulic biaxial device with a torsion cell of ± 1100 Nm. Tests were performed under load control by assuring a nominal load ratio $R=-1$. The frequency ranged between 5 and 20 Hz, as a function of geometry and load level.

In order to carefully analyse the damage mechanics relating to notched specimens, the test were subdivided into a certain number of loading blocks. At the end of each block, the notch was analysed by an optical stereoscope, initially with the aim to check the presence of fatigue cracks and, then, to analyse their propagation. As soon as the fatigue tests were concluded, the notch root and fracture surfaces as well were analysed by means of electronic microscopy.

RESULTS OF THE FATIGUE TESTS

Torsional Stiffness

During torsion fatigue tests, the stiffness (torque to twisting angle ratio, the angle being measured with respect to the specimen ends) was monitored. Figure 3 shows mean trends of the torsional stiffness for the symmetric V-notches specimens. The plots, are normalised with respect either to the initial stiffness value (on the vertical axis) or the number of cycles to failure (on the horizontal axis). The scatter bars, referred to ± 1 standard deviation, are also drawn.

Some preliminary tensile tests were carried out to evaluate yield strength (0.2% offset), ultimate tensile strength σ_u and Young modulus. The relevant mean values are shown in Table 1.

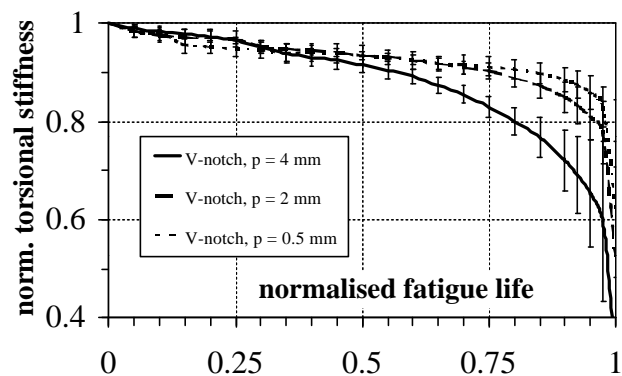


Figure 3. Normalised stiffness trends for V-notched specimens.

It is important to note that, kept constant the notch depth, the stiffness plot does not vary with the load level and, consequently, with the number of cycles to failure. More exactly, the 3 curves show a standard deviation within a 1÷2 % range until 85 percent of fatigue life is spent. On the contrary, the notch dept influences the trend of the stiffness curve: with $p = 4.0$ mm the stiffness is equal to 90% of the initial value at about half of the fatigue life. On the contrary, specimens with $p = 0.5$ mm show a stiffness greater than 90% of the initial value for a number of cycles equal to 85% of the final life. These effects mainly depend on the different value of the net sections. Kept constant the crack depth, the smaller the net section, the more the stiffness reduction is. As shown in Fig. 4, the stiffness variation for the smooth specimens was much more pronounced, in particular at the high stress levels. However, in the fatigue tests the final number of cycles was always referred to complete separation of the specimen.

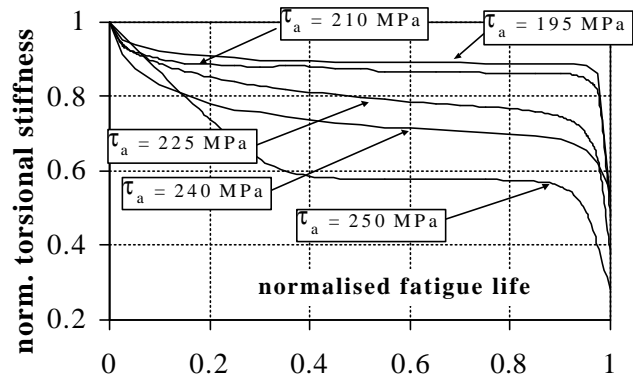


Figure 4. Normalised stiffness trends for smooth specimens.

Fatigue Strength

Table 2 summarises the mean value of the reference shear stress amplitude (on the net area) at $5 \cdot 10^6$ cycles, the slope k and the scatter index relating to the 10-90% probability of survival ($T_\tau = \tau_{A,10\%} / \tau_{A,90\%}$). It is important to note that for the V-notched specimens the high cycle fatigue strength decreases as the notch depth increases. The trend is different from that predicted on the basis of the theoretical stress concentration factor, of which the maximum value was 2.03 for $p = 2$ mm.

Table 2. Results of the torsion fatigue tests ($R = -1$).
Reference shear stress amplitudes at $5 \cdot 10^6$ cycles.

| Series | No. data | $\tau_{A, net 50\%}$ [MPa] | slope k | $T_{\tau,10-90\%}$ |
|-----------------------|----------|----------------------------|-----------|--------------------|
| Smooth | 14 | 186.2 | 18.2 | 1.09 |
| V notch, $p = 0.5$ mm | 7 | 150.7 | 9.9 | 1.07 |
| V notch, $p = 2.0$ mm | 7 | 135.6 | 7.9 | 1.21 |
| V notch, $p = 4.0$ mm | 7 | 126.7 | 7.6 | 1.26 |
| Shaft with shoulders | 8 | 144.2 | 9.1 | 1.05 |

Afterwards, all fatigue strength data have been summarised in term of the mode III Notch Stress Intensity Factor (N-SIF). This factor was evaluated on the uncracked geometries, all the notches being modelled like re-entrant corners (i.e. sharp V-notches).

In particular N-SIFs were evaluated on the bisector of the V-notches ($\theta = 0$), according to the expression:

$$K_3^N = \sqrt{2\pi} \lim_{r \rightarrow 0^+} r^{1-\lambda_3} \cdot \sigma_{\theta z}(r,0) \quad (1)$$

where, for an opening angle equal to $\pi/2$, the eigenvalue λ_3 is equal to $2/3$.

The N-SIF was later correlated to the nominal shear stress according to the following expression

$$\Delta K_3^N = k_3 \Delta \tau_{\text{gross}} p^{1/3} \quad (2)$$

where p is the notch depth. In the case of specimens with shoulders, p was assumed equal to the shoulder height (4.0 mm). The values of the k_3 factors were 5.88, 3.22 and 2.67 for the V notch specimens with notch depth of 4.0, 2.0 and 0.5 mm, respectively, while the specimens with shoulders had $k_3 = 1.33$. With reference to $5 \cdot 10^6$ cycles, the intersection between Eq.(2) and the fatigue strength of the smooth specimens provided the value $p_0 = 0.18$ mm of the "intrinsic" defect under fully-reversed torsion. Since such a value was quite close to the minimum value of the notch depth, p_0 was included into the depth p but only in the case of V-notches with the lowest depth (0.5 mm). The procedure adopted is clearly reminiscent of the method suggested by El Haddad, Smith and Topper to evaluate the material length parameter a_0 [9]

Figure 5 shows all fatigue strength data of notched specimens re-calculated in terms of the N-SIF parameter. It is evident that a band of limited width is able to summarise together all data. The scattered of the band is $T_{K,10-90\%} = 1.2$, even lower than the stress-based scatter pertaining the two series of specimens with $p = 2.0$ and 4.0 mm.

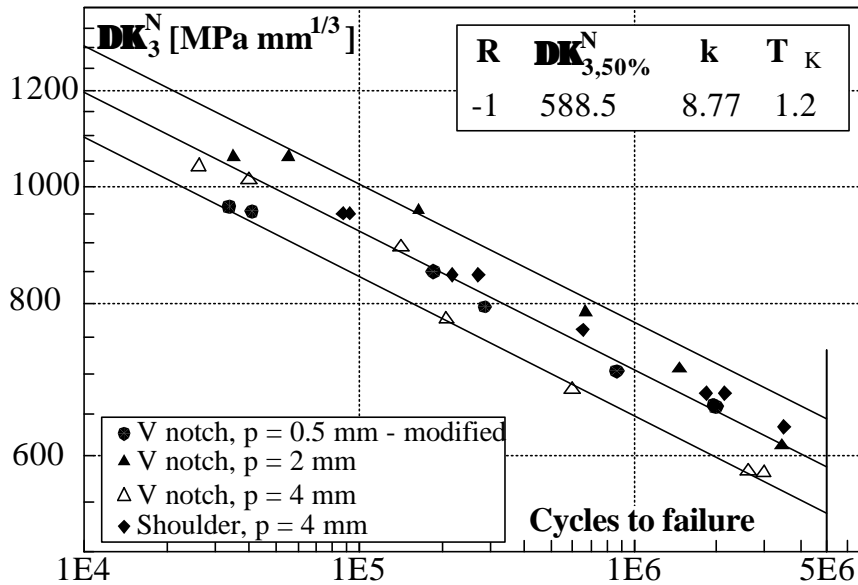


Figure 5. Fatigue strength data re-analysed in terms of the mode III N-SIFs.

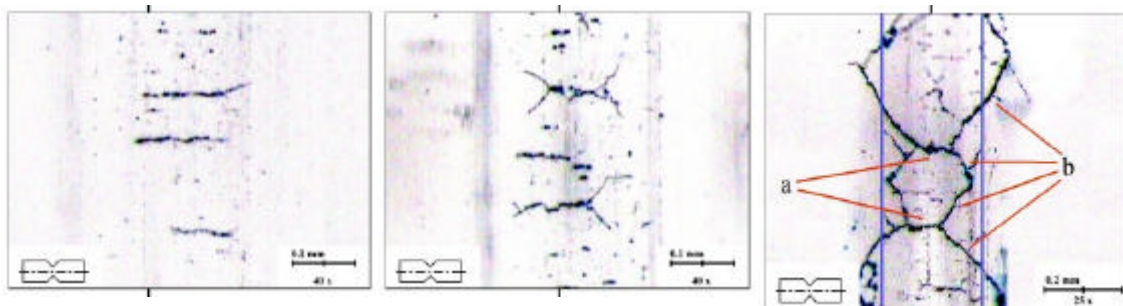
DAMAGE MECHANICS

Crack initiation was observed in the early fraction of the fatigue life: specimens appeared to be cracked before 5 % of the cycles required for the specimen failure. The observation of damage mechanism put in evidence a different strength to crack initiation of the two maximum shear stress planes. In fact, cracks started in the plane aligned with specimen's axis due to the anisotropic microstructure made by alternate bands of ferrite and pearlite already shown in Fig. 2.

Failures at High Number of Cycles

The micrographs reported in Fig. 6 document typical damage patterns for a high cycle fatigue failure. Cracks nucleate before of 5% total life on planes parallel to torsion axis (Fig. 6.1) due to shear stress components. After a short propagation in the direction of the maximum shear stress, cracks change their direction and branch. The new directions are inclined $\pm 45^\circ$ with respect to the previous one (Fig. 6.2) and coincide with the direction of the maximum normal stress. This change of direction is well documented in the literature, with reference to specimens with small superficial notches [6,8], smooth specimens [7], V-notched specimens [2].

Main cause of the phenomenon is the friction present between the surfaces of a crack nucleated on the maximum shear stress plane. The friction decreases the driving force and provokes a reduction of the strains acting on the crack tips. Obviously the friction force increases as the crack length increases until mode III stress component drops below a threshold value. The propagation changes its direction due to the presence of normal stresses. Such stresses tend to separate the crack surfaces, strongly reducing the friction influence.



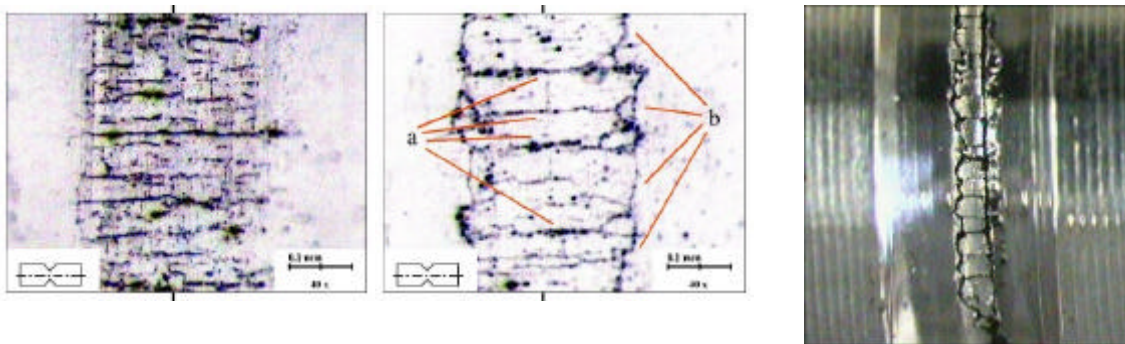
1. cracks nucleated on the planes parallel to the specimen axis (5% of the fatigue life);
2. branching ($\pm 45^\circ$) on the planes of maximum principal stress (10% of the fatigue life);
3. notch root at 70 % of the fatigue life;
4. fracture path at final failure.

Figure 6. Fatigue damage evolution for high cycle fatigue (V-notch $p = 2$ mm, $\tau_{a,nom} = 140$ MPa, $N = 3453000$).



Failures at Low Number of Cycles

The typical damage evolution at low cycle fatigue is shown in Fig. 7. With respect to the case shown in Fig. 6, the number of cracks is now strongly increased and the branching inclined ± 45 degrees is disappeared. The cracks propagate on the initiation planes until they occupy the entire semicircular arc that describes the notch root. Then they stop in correspondence of the two lines where the curved surface of the semicircular arc intersects the inclined flanks of the notch. Afterwards a second phase of propagation begins with a nucleation of cracks on the other (second) plane of maximum shear stress. The plane can be considered normal to the specimen axis (Fig. 7.2), although not exactly coincident with the minimum transverse section.



1. Cracks nucleated on the planes parallel to the specimen axis (28 % of the total fatigue life);
2. Cracks nucleated on the maximum shear stress planes, parallel (a) and normal (b) to the specimens axis (85 % of the fatigue life);
3. Notch root image with fracture surfaces on the plane of maximum shear stress normal to specimen axis (final failure);

Figure 7. Fatigue damage evolution for low cycle fatigue
(V-notch $p = 2$ mm, $\hat{\sigma}_{a,nom} = 240$ MPa, $N = 35274$).

DISCUSSION AND CONCLUSIONS

The nucleation of the cracks on the plane of maximum shear stress parallel to the specimens axis is ascribable to the steel microstructure characterised by alternate bands of ferrite and pearlite oriented along the specimen axis (see Fig. 2).

Local strains measurements carried out by means of SEM analyses [4] demonstrated that the ferritic bands are more susceptible to deformation than pearlitic bands (see Fig. 8).

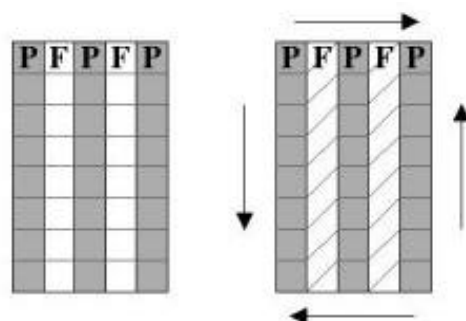


Figure 8. Strain concentration on the ferritic bands.

This results in very localised concentration effects for the strains and, consequently, the nucleation of cracks parallel to the bands, localised either at the phase interface or inside the ferritic bands. As above said, in the low cycle fatigue first cracks were parallel to the specimens axis followed by a number of cracks which nucleate and propagate in the transverse direction on the second plane of maximum shear stress (see Figs 7.1 and 7.2). Therefore, the final fracture surface appears to be substantially normal to the specimen axis, due to the coalescence of cracks propagating on the net transverse section as shown in Fig. 9a.

Under high cycle fatigue conditions, fracture surfaces are very different, exhibiting the typical “factory roof”[2], with a quite small number of surfaces inclined $\pm 45^\circ$ with respect to the specimen axis (see Fig. 9b). Such surfaces are the result of the crack branching and propagation towards the core under normal tensile stresses.



a) $d = 16$ mm V-notch $p = 2$ mm;
 $\hat{\sigma}_{a,nom-net} = 240$ MPa; $N = 35.274$



b) $d = 19$ mm; V-notch $p = 0.5$ mm;
 $\hat{\sigma}_{a,nom-net} = 165$ MPa; $N = 1.979.392$

Figure 9. SEM fracture surfaces under low and high cycle fatigue conditions.

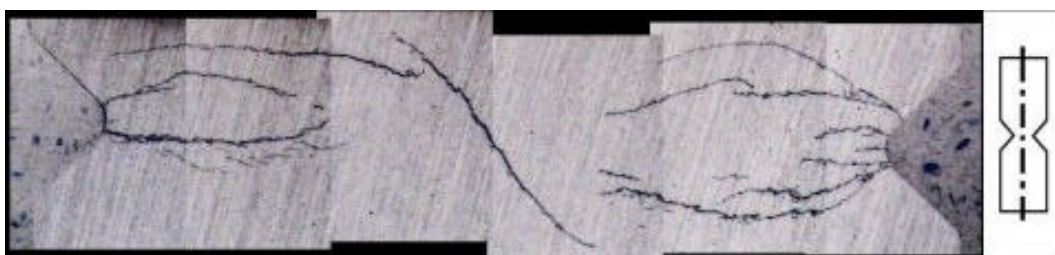


Figure 10. Longitudinal section embracing the V-notch
 ($d = 16$ mm V-notch $p = 2$ mm; $\tau_{a,nom-net} = 160$ MPa; $N = 1.465.000$).

Figure 10 shows crack paths on a longitudinal section of a specimen subjected to high cycle fatigue. On the right and left hand side of the figure is clearly visible the V-shaped notch. The transition between the two fracture modes happens gradually.

More precisely, from low cycle fatigue to high cycle fatigue, nucleation and propagation phases change as illustrated in Fig. 11:

- The distance Δs between the cracks parallel to the specimen axis increases;
- The crack length L before branching decreases. Under the highest load levels, the branching disappears simply because the length L becomes greater than the arc describing the notch root.

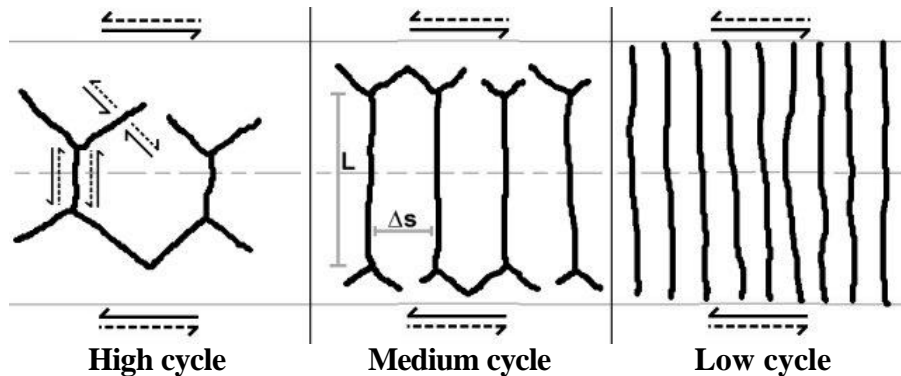


Figure 11. Damage patterns for different fatigue lives (specimen axis thought of as coincident with the vertical direction).

REFERENCES

1. Pook, L.P. (1982) In: *Fatigue thresholds: Fundamentals and Engineering applications*. EMAS Ltd, West Midlands, U.K., pp. 1007-1032
2. Tschegg, E.K. (1983) *Journal of Material Science* **18**, 1604-1614.
3. Yates, J.R. and Miller, K.J. (1989) *Fatigue Fract. Engng Mater. Struct.* **12**, 259-270.
4. Nisitani H., Fukuda, T. (1992) *JSME Int. Journal Series I* **35**, 354-360.
5. Tong, J., Yates, J.R. and Brown, M.W. (1996). *Int J Fatigue* **18**, 279-285.
6. Murakami, Y. and Takahashi, K. (1998). *Fatigue Fract. Engng Mater. Struct.* **21**, 1473-1484.
7. Marquis, G. and Socie, D. F. (2000) *Fatigue Fract. Engng Mater. Struct.* **23**, 293-300.
8. Makabe, C. and Socie, D.F. (2001) *Fatigue Fract. Engng Mater. Struct.* **24**, 607-615.
9. El Haddad, M.H., Topper, T.H. and Smith, K.N. (1979) *Engng Fract. Mech.* **11**, 573-584.